Inorg. Chem. **2008**, *47*, 1815−1823

Forum

Oxygen Evolution Catalysis by a Dimanganese Complex and Its Relation to Photosynthetic Water Oxidation

Ranitendranath Tagore, Robert H. Crabtree,* and Gary W. Brudvig*

Department of Chemistry, Yale University, P.O. Box 208107, New Haven, Connecticut 06520-8107

Received November 21, 2006

$[Mn_2^{III/IV}(\mu\text{-}O)_2(terpy)_2(OH_2)_2](NO_3)_3$ (**1**, where terpy = 2,2′:6′2″-terpyridine) acts as a water-oxidation catalyst with HSO_5^- as the primary oxidant in aqueous solution and, thus, provides a model system for the oxygen-evolving complex of photosystem II (Limburg, J.; et al. *J. Am. Chem. Soc.* **2001**, *123*, 423–430). The majority of the starting $[Mn_2^{III/IV}(\mu\text{-}O)_2]^{3+}$ complex is converted to the $[Mn_2^{IV/IV}(\mu\text{-}O)_2]^{4+}$ form (**2**) during this reaction (Chen, H.; et al. *Inorg. Chem.* **2007**, *46*, 34–43). Here, we have used stopped-flow UV–visible spectroscopy to monitor UV–visible absorbance changes accompanying the conversion of **1** to **2** by HSO_5^-. With excess HSO_5^-, the rate of absorbance change was found to be first-order in [**1**] and nearly zero-order in $[HSO_5^-]$. At relatively low $[HSO_5^-]$, the change of absorbance with time is distinctly biphasic. The observed concentration dependences are interpreted in terms of a model involving the two-electron oxidation of **1** by HSO_5^-, followed by the rapid reaction of the two-electron-oxidized intermediate with another molecule of **1** to give two molecules of **2**. In order to rationalize biphasic behavior at low $[HSO_5^-]$, we propose a difference in reactivity of the $[Mn_2^{III/IV}(\mu\text{-}O)_2]^{3+}$ complex upon binding of HSO_5^- to the Mn^{III} site as compared to the reactivity upon binding HSO_5^- to the Mn^{IV} site. The kinetic distinctness of the Mn^{III} and Mn^{IV} sites allows us to estimate upper limits for the rates of intramolecular electron transfer and terminal ligand exchange between these sites. The proposed mechanism leads to insights on the optimization of **1** as a water-oxidation catalyst. The rates of terminal ligand exchange and electron transfer between oxo-bridged Mn atoms in the oxygen-evolving complex of photosystem II are discussed in light of these results.

Introduction

The oxygen-evolving complex (OEC) of photosystem II consists of manganese ions connected by μ-oxo linkages[1] and catalyzes the oxidation of water to molecular oxygen. Synthetic manganese compounds have been studied extensively as models of the OEC, with an abundance of structurally relevant complexes.[2] However, functional analogy to the OEC has only been rarely achieved with manganese. Instead, ruthenium has provided the first examples of homogeneous water-oxidation catalysts. The complexes $[(bpy)_2(H_2O)Ru^{III}ORu^{III}(H_2O)(bpy)_2]^{4+}$ (bpy = 2,2′-bipyridine) and $[(phen)_2(H_2O)Ru^{III}ORu^{III}(H_2O)(phen)_2]^{4+}$ (phen = 1,10-phenanthroline) were reported in 1982 by Meyer et al. to catalyze oxygen evolution via water oxidation in the presence of Ce^{4+}.[3,4] These complexes were shown to retain their oxo-bridged structures in the II/II, III/III, III/IV, IV/IV, IV/V, and V/V oxidation states, leading to the existence of extensive redox chemistry.[4–7] Mechanistic studies[5–12] have implicated the V/V oxidation state, formulated as $[Ru^V{\equiv}O]_2O$, as the oxygen-evolving species. At-

* To whom correspondence should be addressed. E-mail: gary.brudvig@yale.edu (G.W.B.), robert.crabtree@yale.edu (R.H.C.).

(1) Kirby, J. A.; Robertson, A. S.; Smith, J. P.; Thompson, A. C.; Cooper, S. R.; Klein, M. P. *J. Am. Chem. Soc.* **1981**, *103*, 5529–5537.
(2) Mukhopadhyay, S.; Mandal, S. K.; Bhaduri, S.; Armstrong, W. H. *Chem. Rev.* **2004**, *104*, 3981–4026.
(3) Gersten, S. W.; Samuels, G. J.; Meyer, T. J. *J. Am. Chem. Soc.* **1982**, *104*, 4029–4030.
(4) Gilbert, J. A.; Eggleston, D. S.; Murphy, W. R.; Geselowitz, D. A.; Gersten, S. W.; Hodgson, D. J.; Meyer, T. J. *J. Am. Chem. Soc.* **1985**, *107*, 3855–3864.
(5) Lei, Y.; Hurst, J. K. *Inorg. Chim. Acta* **1994**, *226*, 179–185.
(6) Lei, Y.; Hurst, J. K. *Inorg. Chem.* **1994**, *33*, 4460–4467.
(7) Yamada, H.; Hurst, J. K. *J. Am. Chem. Soc.* **2000**, *122*, 5303–5311.
(8) Binstead, R. A.; Chronister, C. W.; Ni, J.; Hartshorn, C. M.; Meyer, T. J. *J. Am. Chem. Soc.* **2000**, *122*, 8464–8473.

10.1021/ic062218d CCC: $40.75
Published on Web 03/10/2008

tempts to optimize water-oxidation catalysis have led to a series of complexes, reviewed by Hurst,[12] involving modifications to the structure of the parent Ru-bpy and Ru-phen complexes. These include substitution on the bpy ligand,[13,14] use of the tridentate terpy (2,2′:6′2″-terpyridine) ligand instead of two bpy ligands,[15] and use of the bridging ligand 3,5-bis(pyridinyl)pyrazole in place of the oxo bridge.[16]

Water-oxidizing manganese systems include a phenylene-bridged $Mn_2^{III/III}$ porphyrin dimer, which has been shown to form a $(Mn^{V}{=}O)_2$ dimer upon oxidation with *m*-chloroperbenzoic acid under basic conditions.[17] The oxo ligands in this porphyrin dimer point into the hydrophobic cavity formed by the porphyrin rings and are, thus, sterically protected. Acidification of the $(Mn^{V}{=}O)_2$ dimer leads to the regeneration of the $Mn_2^{III/III}$ dimer via water oxidation. Isotope-labeling experiments demonstrate the quantitative incorporation of O atoms from water into the evolved O_2. Thus, this bis(porphyrin) system constitutes a potentially catalytic water-oxidation system. A Mn_4O_4 cubane-like complex has been reported to release its bridging oxides as water upon reduction[18] and as O_2 upon photoexcitation in the gas phase,[19] thus being a potential functional model for the OEC requiring the combination of the two separate reactions into one catalytic cycle. To date, however, only two structurally relevant inorganic manganese complexes have been reported to catalyze homogeneous water oxidation with catalytic turnover.

A bis(carboxylate)-bridged $Mn_2^{II/II}$ dimer has been reported to catalyze water oxidation via the formation of higher valent oxo-bridged dimers in situ when *tert*-butylhydrogen peroxide is used as the primary oxidant.[20] The proposed mechanism involves the oxidative cleavage of the $Mn_2^{II/II}$ dimer into Mn^{III} monomers, followed by the formation of di-μ-oxo-bridged species. The oxo bridges are proposed to be released as O_2 via the intermediate formation of a bridging peroxo species.

The other manganese-based water-oxidation catalyst, $[(H_2O)(terpy)Mn^{III}(\mu\text{-}O)_2Mn^{IV}(terpy)(H_2O)]^{3+}$ (**1**),[21] was reported by our group to produce O_2 catalytically with oxone ($2KHSO_5 \cdot KHSO_4 \cdot K_2SO_4$)[22,23] or NaOCl[21,23] as primary oxidants. Catalysis of the oxygen evolution by **1** shows first-order kinetics with respect to **1** and saturation (Michaelis–Menten-like) kinetics with respect to either HSO_5^- or ClO^- as the oxidant, indicating similar mechanisms in both cases. However, the catalysis is more efficient and robust with HSO_5^- [$V_{max} = 2420 \pm 490$ mol of O_2 (mol of **1**)$^{-1}$ h^{-1}, $K_M = 53 \pm 5$ mM for [**1**] = 7.5 μM, and >50 mol of O_2 evolved per 1 mol of **1**] than with ClO^- [$V_{max} = 6.5 \pm 0.3$ mol of O_2 (mol of **1**)$^{-1}$ h^{-1}, $K_M = 39 \pm 4$ mM for [**1**] = 70 μM, and ~5 mol of O_2 evolved per 1 mol of **1**).[23] In comparison, the only other reported case of homogeneous water oxidation with catalytic turnover by a manganese complex[20] is the oxygen-evolving reaction catalyzed by the carboxylate-bridged $Mn_2^{II/II}$ dimer described above,[24] which produces ~6 mol of O_2 per 1 mol of the catalyst over the course of ~3 h when *tert*-butylhydrogen peroxide is used as the primary oxidant.

Oxygen-evolution catalysis by **1** has been the subject of study by groups other than our own. While some authors have independently confirmed oxygen-evolution catalysis by **1** and related complexes,[25,26] others have debated the source of oxygen evolution.[27,28] Isotope-labeling studies and comparisons of the activities of a series of complexes provide strong evidence for water oxidation by a high-valent multinuclear manganese species. We have observed isotopic enrichment of evolved O_2 in the presence of isotopically enriched water.[21,23,29] This observation alone does not prove the oxidation of the O atoms in water to O_2 because it is possible that the O atoms of water can exchange with other oxygen-containing species in the system. Subsequent oxidation of such oxygen-containing species could then produce isotopically enriched oxygen without involving the oxidation of water by high-valent manganese. Therefore, in order to prove that water oxidation is the source of oxygen evolution, it must be demonstrated that exchange of O atoms between water and other oxygen-containing species cannot account for the observed isotopic enrichment. In the oxygen-evolving system **1** + HSO_5^-, it was shown that water does not undergo O atom exchange with the oxidant HSO_5^-, the SO_4^{2-} ions present along with HSO_5^-, or with the NO_3^- counterions of **1**. Electrospray ionization mass spectrometry (ESI-MS) spectra of these species under catalytic conditions show no isotopic exchange, clearly demonstrating that oxidation of these species cannot account for isotopic enrichment of the evolved oxygen.[29] The extent of isotopic enrichment shows a direct dependence on [$H_2{}^{18}O$] and an inverse dependence

(9) Chronister, C. W.; Binstead, R. A.; Ni, J.; Meyer, T. J. *Inorg. Chem.* **1997**, *36*, 3814–3815.
(10) Geselowitz, D.; Meyer, T. J. *Inorg. Chem.* **1990**, *29*, 3894–3896.
(11) Hurst, J. K.; Zhou, J.; Lei, Y. *Inorg. Chem.* **1992**, *31*, 1010–1017.
(12) Hurst, J. K. *Coord. Chem. Rev.* **2005**, *249*, 313–328.
(13) Comte, P.; Nazeeruddin, M. K.; Rotzinger, F. P.; Frank, A. J.; Grätzel, M. *J. Mol. Catal.* **1989**, *52*, 63–84.
(14) Rotzinger, F. P.; Munavalli, S.; Comte, P.; Hurst, J. K.; Graetzel, M.; Pern, F. J.; Frank, A. J. *J. Am. Chem. Soc.* **1987**, *109*, 6619–6626.
(15) Lebeau, E. L.; Adeyemi, S. A.; Meyer, T. J. *Inorg. Chem.* **1998**, *37*, 6476–6484.
(16) Sens, C.; Romero, I.; Rodriguez, M.; Llobet, A.; Parella, T.; Benet-Buchholz, J. *J. Am. Chem. Soc.* **2004**, *126*, 7798–7799.
(17) Shimazaki, Y.; Nagano, T.; Takesue, H.; Ye, B.-H.; Tani, F.; Naruta, Y. *Angew. Chem., Int. Ed.* **2004**, *43*, 98–100.
(18) Ruettinger, W. F.; Dismukes, G. C. *Inorg. Chem.* **2000**, *39*, 1021–1027.
(19) Ruettinger, W.; Yagi, M.; Wolf, K.; Bernasek, S.; Dismukes, G. C. *J. Am. Chem. Soc.* **2000**, *122*, 10353–10357.
(20) Poulsen, A. K.; Rompel, A.; McKenzie, C. J. *Angew. Chem., Int. Ed.* **2005**, *44*, 6916–6920.
(21) Limburg, J.; Vrettos, J. S.; Liable-Sands, L. M.; Rheingold, A. L.; Crabtree, R. H.; Brudvig, G. W. *Science* **1999**, *283*, 1524–1527.
(22) Limburg, J.; Brudvig, G. W.; Crabtree, R. H. *J. Am. Chem. Soc.* **1997**, *119*, 2761–2762.
(23) Limburg, J.; Vrettos, J. S.; Chen, H.; de Paula, J. C.; Crabtree, R. H.; Brudvig, G. W. *J. Am. Chem. Soc.* **2001**, *123*, 423–430.
(24) Baffert, C.; Collomb, M.-N.; Deronzier, A.; Kjærgaard-Knudsen, S.; Latour, J.-M.; Lund, K. H.; McKenzie, C. J.; Mortensen, M.; Nielsen, L. P.; Thorup, N. *Dalton Trans.* **2003**, *1765*, 1772.
(25) Wolpher, H.; Huang, P.; Borgstroem, M.; Bergquist, J.; Styring, S.; Sun, L.; Akermark, B. *Catal. Today* **2004**, *98*, 529–536.
(26) Hammarstrom, L. *Personal communication*, **2007**.
(27) Baffert, C.; Romain, S.; Richardot, A.; Leprêtre, J.-C.; Lefebvre, B.; Deronzier, A.; Collomb, M.-N. *J. Am. Chem. Soc.* **2005**, *127*, 13694–13704.
(28) Yagi, M.; Narita, K. *J. Am. Chem. Soc.* **2004**, *126*, 8084–8085.
(29) Chen, H.; Tagore, R.; Olack, G.; Vrettos, J. S.; Weng, T.-C.; Penner-Hahn, J.; Crabtree, R. H.; Brudvig, G. W. *Inorg. Chem.* **2007**, *46*, 34–43.

Scheme 1. Proposed Mechanism for the Reaction between **1** and Oxygen-Atom Transfer Reagents, XO, According to Reference 23

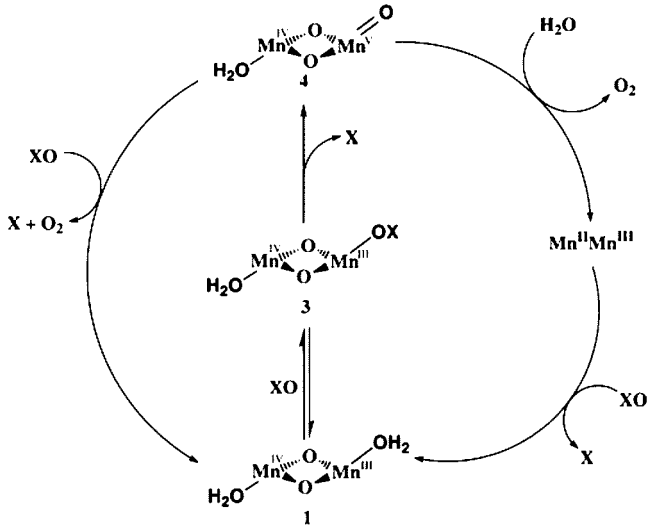

on [HSO_5^-], demonstrating the existence of a pathway involving the formation of O_2 from water without prior exchange of oxygen from water with the oxygens of HSO_5^-.[23,29]

Elucidation of the nature of the species catalyzing water oxidation is central to any claim of structural and functional relevance to the OEC. Toward this end, we have shown that non-redox-active Lewis acids do not catalyze oxygen evolution with HSO_5^-, demonstrating that the active catalyst requires redox activity.[22,23,29] We have also shown that the products of decomposition of **1** are not the active catalysts for O_2 evolution.[29] Moreover, the rate of oxygen evolution from a solution of **1** + HSO_5^- correlates with the concentration of the $Mn_2^{III/IV}$ form of **1**.[29]

On the basis of isotope-labeling studies, kinetic behavior, and the known reactivity of terminal metal−oxo species, the native $Mn_2^{III/IV}$ form of **1** is proposed to be the precursor to a water-oxidizing species containing Mn^V═O (Scheme 1).[23,29] Consistent with this proposal, the concentration of $Mn_2^{III/IV}$ in solution is maintained at low steady-state levels (∼2–5% of the total manganese) during catalysis and the concentration of $Mn_2^{III/IV}$ correlates with the catalytic activity.[29] The mixed-valent $Mn_2^{III/IV}$ species is regenerated in ∼75% yield when O_2 evolution ceases because of the depletion of HSO_5^-. The major manganese species under steady-state conditions is the $Mn_2^{IV/IV}$ form of the dimer (**2**), which is catalytically inactive with HSO_5^-. The lack of catalytic activity by the $Mn_2^{IV/IV}$ species has been attributed to the obligated two-electron redox chemistry of HSO_5^- in conjunction with the inaccessibly high potential required to form the $Mn_2^{V/V}$ redox state of **1**. The $Mn_2^{IV/IV}$ oxidation state is, however, likely to participate in the water-oxidation pathway in the presence of the one-electron oxidant Ce^{4+}, although the acidic conditions associated with the use of Ce^{4+} prevents catalytic turnover.[30]

In this study, we investigate the formation of $Mn_2^{IV/IV}$ (**2**) from $Mn_2^{III/IV}$ (**1**) in the presence of HSO_5^- by stopped-flow UV–visible absorption spectroscopy. As noted above, **2** is the major manganese species in solution under steady-state conditions in the presence of excess HSO_5^- but is catalytically inactive under these conditions. Preventing the conversion of **1** to **2** could, therefore, provide a strategy for better catalyst design when using two-electron oxidants such as HSO_5^-. The observation of saturation kinetics in the reaction of HSO_5^- with **1** suggests a unimolecular rate-determining reaction of the HSO_5^--bound form of **1**. This is consistent with the rate-determining transfer of oxidizing equivalents from the HSO_5^- moiety to manganese, leading to the formation of a high-valent manganese dimer containing a Mn^V═O (or $Mn^{IV}-O^{\bullet}$) species.[23,29] In the present study, the biphasic nature of the time course of absorbance change in the reaction of **1** with HSO_5^- indicates the existence of two kinetically distinct forms of **1**. These are proposed to differ in the site of binding of HSO_5^- on **1** (Mn^{III} vs Mn^{IV}). Kinetic distinctness of the oxone-bound Mn^{III} and Mn^{IV} sites implies that ligand exchange and intramolecular electron transfer between the manganese sites in **1** in the presence of oxone is slow, on the millisecond time scale. This is consistent with the classification of the analogous complex $[(bpy)_2Mn^{III}(\mu\text{-}O)_2Mn^{IV}(bpy)_2]^{3+}$ (**3**) as a "deeply trapped" mixed-valent complex[31] and with the calculated barriers to intramolecular electron transfer[32] and terminal ligand exchange on the Mn^{IV} site[33] in $Mn^{III}(\mu\text{-}O)_2Mn^{IV}$ complexes.

Experimental Section

Materials. Solutions of **1** and oxone were made in a 0.1 M NaOAc buffer adjusted to pH 4.5 with HOAc. **1** was synthesized according to a literature procedure.[21] Oxone ($2KHSO_5 \cdot KHSO_4 \cdot K_2SO_4$) was purchased from Acros Organics and standardized for HSO_5^- content by the addition of a known excess of KI, followed by titration of the liberated I_2 with a standard $Na_2S_2O_3$ solution using starch as the indicator. NaOAc and HOAc were purchased from Sigma Aldrich and J.T. Baker, respectively.

UV–Visible Spectroscopy. Stopped-flow UV–visible spectra were recorded on a Kintek SF-2001 spectrometer. Syringes containing the reactant solutions were maintained at 25 °C in a water bath. Multiple-wavelength spectra were acquired every 9 ms using a CCD array detector. Absorbance readings were normalized to a path length of 1 cm by the acquisition software. For single-wavelength kinetic analysis, the time courses of absorbance changes at 425 and 530 nm were used because the molar extinction coefficients of **1** and **2** are significantly different at these wavelengths. Moreover, the choice of these two wavelengths allowed analysis at two different concentration ranges of manganese because both **1** and **2** absorb much more strongly at 425 nm than at 530 nm. Non-time-resolved spectra were acquired on a Varian Cary-50 UV–visible spectrophotometer at room temperature using a 1 cm path-length cuvette.

Kinetic Simulations. Simulations of kinetic schemes were performed with the help of the DYNAFIT software,[34] version 3.28.038, available free of charge via the Internet for academic users at http://www.biokin.com/dynafit.

(30) Tagore, R.; Chen, H.; Zhang, H.; Crabtree, R. H.; Brudvig, G. W. *Inorg. Chim. Acta* **2007**, *360*, 2983–2989.
(31) Cooper, S. R.; Dismukes, G. C.; Klein, M. P.; Calvin, M. *J. Am. Chem. Soc.* **1978**, *100*, 7248–7252.
(32) Lundberg, M.; Siegbahn, P. E. M. *J. Phys. Chem. B* **2005**, *109*, 10513–10520.
(33) Lundberg, M.; Blomberg, M. R. A.; Siegbahn, P. E. M. *Theor. Chem. Acc.* **2003**, *110*, 130–143.

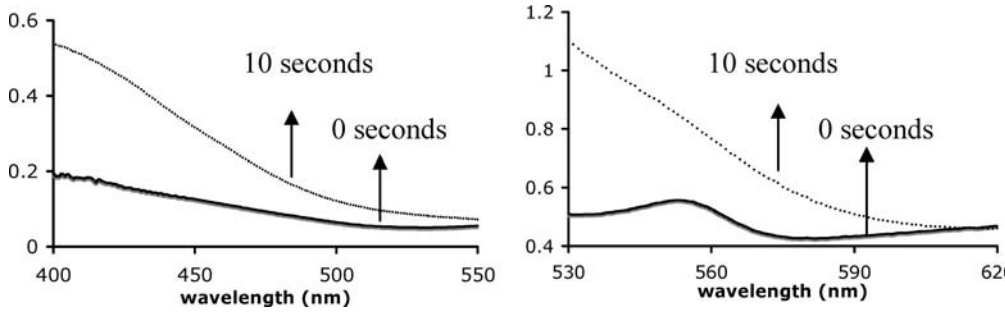

Figure 1. Visible absorption changes upon the reaction of 15 mM HSO_5^- with 75 μM **1** (left panel) and 0.75 mM **1** (right panel).

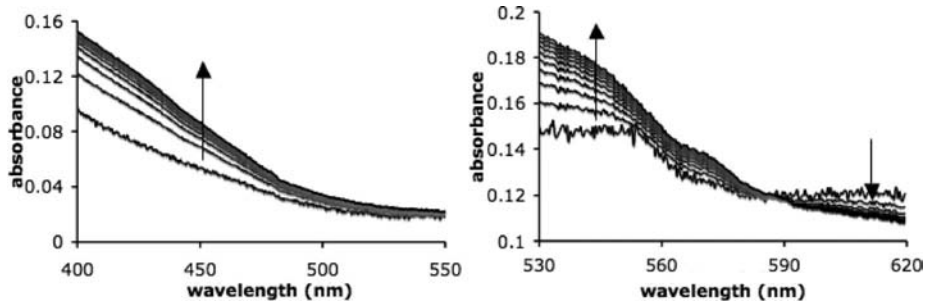

Figure 2. Stopped-flow absorption spectra of the reaction of 15 mM HSO_5^- with 30 μM **1** (left panel) and 200 μM **1** (right panel). Spectra were recorded every 9 ms from the time of mixing up to 2.15 s. For the sake of clarity, every 26th spectrum, starting from the first, is shown. Arrows show the direction of the absorbance change with time.

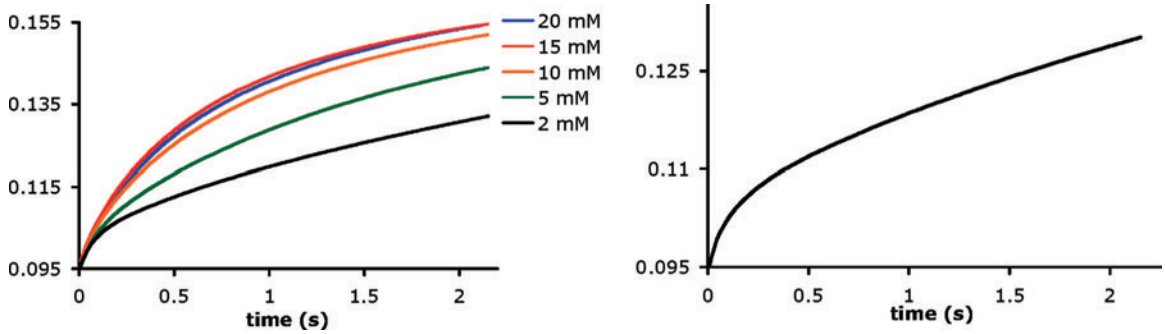

Figure 3. Representative time courses of absorbance changes at 425 nm upon the reaction of 30 μM **1** with varying concentrations of HSO_5^-. The right panel shows an enlarged view of the biphasic trace for 2 mM HSO_5^-.

Results

Changes in the UV–Visible Spectrum of 1 upon the Addition of Oxone. Figure 1 shows the absorption spectra of **1** before and 10 s after the addition of oxone. The changes in the absorption spectra were time-resolved by stopped-flow UV–visible spectroscopy (Figure 2). Changes in the lower wavelength region (~400–450 nm) were monitored at lower concentrations of **1** (15–75 μM), while changes around 550 nm were suitable for experiments with higher concentrations ($\geq$100 μM).

Concentration Dependence. Stopped-flow data were acquired at a number of concentrations of **1** and oxone. Control experiments did not show any dependence on $[SO_4^{2-}]$, so that we use the term $[HSO_5^-]$ as the relevant variable instead of [oxone] from here onward. From the concentration-dependence data, the absorption changes at 425 nm (Figure 3) and 530 nm (not shown) were plotted against time. The absorption changes show a markedly biphasic character when $[HSO_5^-] \leq 5$ mM and monophasic single-exponential character at higher concentrations. This behavior is seen at both high and low concentrations of **1** (200 and 30 μM, respectively). The initial linear parts of the single-wavelength data were used to calculate the dependence of initial rates on [**1**] and $[HSO_5^-]$. The initial rates showed a weak ~0.2-order dependence on $[HSO_5^-]$ and a first-order dependence on [**1**] (Figure 4).

Discussion

Our previous work on the characterization of the reaction between **1** and oxone[29] has shown that: (1) **1** is converted to an electron paramagnetic resonance (EPR)-silent form in less than 30 s, (2) almost all of the manganese is in the 4+ oxidation state ~1 s after mixing with oxone, and (3) the EPR-silent Mn^{IV} compound is mostly $[(terpy)_2Mn_2^{IV/IV}O_2]^{4+}$. In the current work, therefore, we interpret the changes in

(34) Kuzmic, P. *Anal. Biochem.* **1996**, *237*, 260–273.

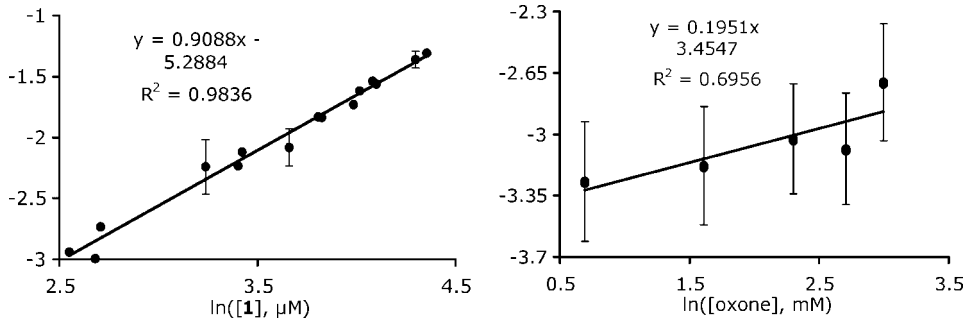

Figure 4. Dependence of the initial rates of the absorbance change in the reaction of **1** with HSO_5^- upon the concentrations of **1** and HSO_5^-. Left panel: Double-logarithmic plot of the rate of the absorbance change at 425 nm as a function of the initial [**1**] for $[HSO_5^-] = 15$ mM. Each data point is the average of 10 runs. Representative error bars are shown to indicate 1 standard deviation about the mean. The linear fit to the data points has a slope of 0.91 ± 0.03. Right panel: Double-logarithmic plot of the rate of the absorbance change at 530 nm as a function of the initial $[HSO_5^-]$ for [**1**] = 200 μM. Error bars indicate 1 standard deviation about the mean of 10 runs. The linear fit to the data points has a slope of 0.20 ± 0.07.

the absorption spectrum as being due to the conversion of $Mn_2^{III/IV}$ (**1**) to $Mn_2^{IV/IV}$ (**2**) by HSO_5^-, as described by eq 1.

$$2Mn_2^{III/IV} + HSO_5^- + H^+ \rightarrow 2Mn_2^{IV/IV} + SO_4^{2-} + H_2O \quad (1)$$

Concentration Dependence. HSO_5^- is widely employed as a two-electron oxidant[35] and is known to suppress radical chemistry.[36] To the best of our knowledge, there are no cases of single-electron-oxidation chemistry with HSO_5^-. The one-electron conversion of **1** to **2** by HSO_5^- is, therefore, expected to be a multistep process. In the present case, a single-step termolecular reaction, as shown in eq 1, is ruled out by the observed first-order dependence of the initial rates on [**1**] and the near-zero dependence on $[HSO_5^-]$.

We, therefore, consider the multistep process where the encounter of a single molecule of **1** with a molecule of HSO_5^- produces an intermediate, which can subsequently react with a second molecule of **1** to give **2**. This scenario can be expressed as in Scheme 2. HSO_5^- binds to one of the labile coordination sites[21] on a molecule of $L_2Mn_2^{III/IV}$ to give the HSO_5^--bound intermediate $L(HSO_5)Mn_2^{III/IV}$, displacing the initially bound ligand, L (eq 2). In an aqueous solution of **1** and oxone in an acetate buffer, L is likely to be water, SO_4^{2-}, or CH_3COO^-. The conversion of the broad EPR signal of **1** in water to a 16-line EPR signal in the presence of CH_3COO^- suggests that $L = CH_3COO^-$ in an acetate-buffered solution.[29] The HSO_5^--bound intermediate further undergoes reaction with another molecule of **1** to give two molecules of **2** (eq 3).

Scheme 2. Reaction Scheme for the Formation of **2** via Oxidation of **1** by HSO_5^-, in Which "L" Denotes the Ligand on the Labile Sixth Coordination Site on Each of the Manganese Ions in **1**, Most Likely CH_3COO^- (See the Text)

$$L_2Mn_2^{III/IV} + HSO_5^- \rightleftharpoons L(HSO_5)Mn_2^{III/IV} + L \quad (2)$$

$$L(HSO_5)Mn_2^{III/IV} + L_2Mn_2^{III/IV} \rightarrow L(OH)Mn_2^{IV/IV} + L_2Mn_2^{IV/IV} + SO_4^{2-} \quad (3)$$

According to this model, the initial reaction rates would show a first-order dependence on both [**1**] and $[HSO_5^-]$ if eq 2 were rate-determining. Alternatively, if eq 3 were rate-determining, then the initial rates would show a second-order dependence on [**1**] and a zero-order dependence on $[HSO_5^-]$. In the intermediate case, the dependence would be between first and second order on [**1**] and between zero and first order on $[HSO_5^-]$. Our attempts to simulate this behavior according to Scheme 2 were not successful; optimization to yield the correct dependence on [**1**] led to the simulation of too high of a dependence on $[HSO_5^-]$, while optimization for the correct dependence on $[HSO_5^-]$ predicted too high of a dependence on [**1**]. Thus, we considered the alternative scheme described below.

Two-Electron Oxidation of $[Mn_2^{III/IV}(\mu\text{-}O)_2]^{3+}$. Rate-determining reactions between manganese dimer molecules are ruled out by the observed first-order dependence of the initial rate on [**1**]. The dependence of the initial rate on $[HSO_5^-]$ implies that HSO_5^- enters the reaction at, or prior to, the rate-determining step. The rate-determining unimolecular reaction of a HSO_5^--bound dimer satisfies these requirements. Assuming a favorable binding equilibrium and noting that HSO_5^- is in excess in our experiments, an increase in [**1**] would produce a proportionate increase in the concentration of the HSO_5^--bound dimer, accounting for the first-order dependence on [**1**]. However, if most of the dimer is HSO_5^--bound at even the lowest HSO_5^- concentration, then an increase in $[HSO_5^-]$ would not lead to a proportionate increase in the HSO_5^--bound dimer. This would account for the weak dependence on $[HSO_5^-]$. These features are incorporated in Scheme 3, where the first step is the binding of oxone to **1**, as shown in eq 2. The oxone-bound intermediate then undergoes a unimolecular conversion to a species X that is two units more oxidized than **1** and a molecule of SO_4^{2-} (eq 4). The species X then reacts with another molecule of **1** to give two molecules of $Mn_2^{IV/IV}$ (eq 5).

Scheme 3. Reaction Scheme for the Formation of **2** via the Oxidation of **1** by HSO_5^-, with Intermediate Formation of a Two-Electron Oxidation Product of **1**, Denoted as "X", in Which "L" Denotes the Ligand on the Labile Sixth Coordination Site on Each of the Manganese Ions in **1**, Most Likely CH_3COO^- (See the Text)

$$L_2Mn_2^{III/IV} + HSO_5^- \rightleftharpoons L(HSO_5)Mn_2^{III/IV} + L \quad (2)$$

$$L(HSO_5)Mn_2^{III/IV} \rightarrow X + SO_4^{2-} + H^+ \quad (4)$$

$$X + L_2Mn_2^{III/IV} \rightarrow 2L_2Mn_2^{IV/IV} \quad (5)$$

According to Scheme 3, a first-order dependence on [**1**] and a zero-order dependence on $[HSO_5^-]$ would be produced

Scheme 4. Proposed Difference in the Reactivity of **1** with Oxone Bound to the Mn^{III} Site (**1a**) As Compared to That of **1** with Oxone Bound on the Mn^{IV} Site (**1b**)

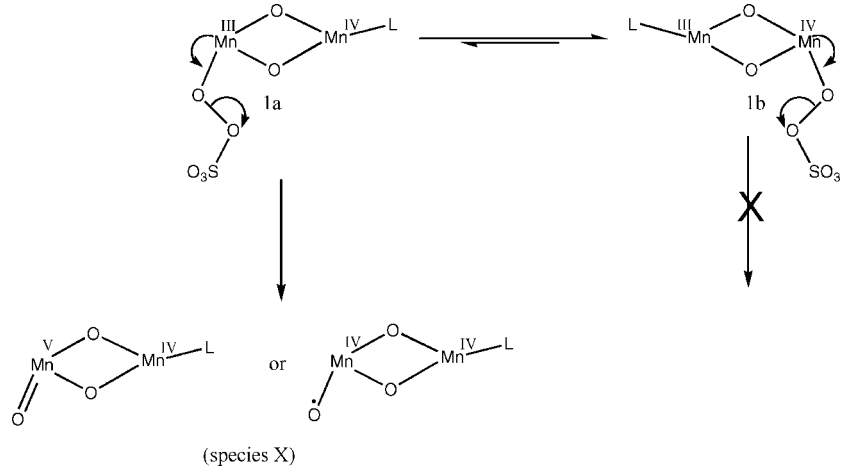

if eq 4 were the rate-determining step. This scheme is consistent with our previously proposed mechanism for oxygen evolution from aqueous solutions of **1** and oxone, where X was formulated as a Mn^{V}═O species, which reacted with water or oxone to evolve O_2 (Scheme 1).[21] An alternative formulation for species X is a Mn^{IV}−O• oxyl radical species.[37] These formulations differ only in the description of electron distribution between the O and Mn atoms. In either case, the reaction of X with water or HSO_5^- leads to the catalytic oxygen evolution pathway, while the reaction with another molecule of **1** leads to the formation of the inactive **2**. Because we could successfully simulate the observed concentration dependences with Scheme 3, we refined it further to reproduce the observed biphasic absorption changes at low [HSO_5^-] and the transition to monophasic behavior at higher [HSO_5^-].

Biphasic Kinetics. We interpret the biphasic absorption changes in terms of the availability of two distinct binding sites for HSO_5^- on **1**. In terms of Scheme 3, binding of HSO_5^- on the Mn^{III} site can lead directly to the formation of species X. On the other hand, an analogous reaction on the Mn^{IV} site would lead to the formation of an unstable Mn^{VI} or Mn^{V}−O• center. Thus, a molecule of **1** with HSO_5^- bound on the Mn^{IV} site (**1b**) has to reconvert to the form with HSO_5^- bound on Mn^{III} (**1a**), either via electron transfer between the manganese centers or via ligand substitution, before the formation of X can occur (Scheme 4).

To explain the biphasic formation of **2**, we make the following assumptions: (1) The equilibrium constant for HSO_5^- substitution on Mn^{IV} is favorable, (2) the equilibrium constant for HSO_5^- substitution on Mn^{IV} to form **1b** is greater than that on Mn^{III} to form **1a**, and (3) the rate of interconversion between **1a** and **1b** is slower than the rate of formation of the intermediate X. These assumptions seem reasonable because Mn^{IV} is expected to be more electrophilic and the $Mn_2^{III/IV}$ complexes show large structural changes between the two metal sites, a factor that is expected to lead to slow electron exchange between the sites. As a consequence of the first and second assumptions, there will be a range of HSO_5^- concentrations where the Mn^{IV} sites will be saturated with HSO_5^- but not the Mn^{III} sites and there will be very small amounts of **1** with no HSO_5^- bound. Under these conditions, the first phase of the reaction will be the conversion of molecules of **1a** to **2** via X. After this, the rate of formation of **2** will be limited by the rate of conversion of **1b** to **1a**. This would constitute the second

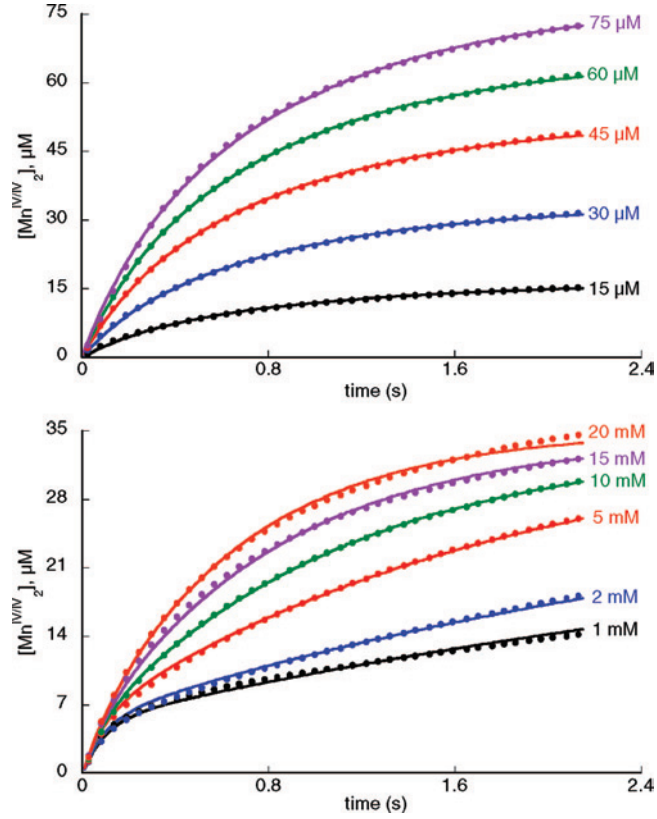

Figure 5. Simulation of experimental data according to Scheme 5. Absorbances measured at 425 nm are converted to [**2**] (see the text) and plotted on the *y* axis. Lines through the experimental data points represent the simulated time course of [**2**]. Top panel: [HSO_5^-] = 15 mM. The initial [**1**] corresponding to each trace is indicated on the graph. Bottom panel: initial [**1**] = 30 μM. The initial [HSO_5^-] corresponding to each trace is indicated on the graph.

(35) Travis, B. R.; Sivakumar, M.; Hollist, G. O.; Borhan, B. *Org. Lett.* **2003**, *5*, 1031–1034.
(36) Wessel, J.; Crabtree, R. H. *J. Mol. Catal. A* **1996**, *113*, 13–22.

phase of the reaction. This biphasic behavior would not be exhibited at higher concentrations of oxone when both manganese sites are saturated with HSO_5^-.

Scheme 5 incorporates these features. The redox changes implied in Scheme 5 are the same as those in Scheme 3. In contrast to Scheme 3, however, Scheme 5 distinguishes between the labile ligand sites (L) on Mn^{III} versus Mn^{IV}. Only the species with a HSO_5^- bound on Mn^{III} are considered to undergo manganese oxidation to give the species X. Thus, $(HSO_5)Mn^{III}Mn^{IV}L$ and $(HSO_5)Mn^{III}Mn^{IV}(HSO_5)$ can convert to X (eqs 7a and 7b), while $LMn^{III}Mn^{IV}L$ and $LMn^{III}Mn^{IV}(HSO_5)$ cannot. Any of the species $LMn^{III}Mn^{IV}L$, $(HSO_5)Mn^{III}Mn^{IV}L$, $LMn^{III}Mn^{IV}(HSO_5)$, and $(HSO_5)Mn^{III}Mn^{IV}(HSO_5)$ can subsequently react with X to give **2**. The ligands on the labile sites of **2** are not specified because that will depend on the ligands on X and its reaction partner in eqs 8a−8d.

Scheme 5. Expansion of Scheme 3, As Adapted from Scheme 4, To Distinguish between Binding of HSO_5^- to the Mn^{III} and Mn^{IV} Sites of **1**

$$LMn^{III}Mn^{IV}L + HSO_5^- \underset{k_{-3}}{\overset{k_3}{\rightleftharpoons}} (HSO_5)Mn^{III}Mn^{IV}L + L \quad (6a)$$

$$LMn^{III}Mn^{IV}L + HSO_5^- \underset{k_{-4}}{\overset{k_4}{\rightleftharpoons}} LMn^{III}Mn^{IV}(HSO_5) + L \quad (6b)$$

$$(HSO_5)LMn^{III}Mn^{IV}L + HSO_5^- \underset{k'_{-4}}{\overset{k'_4}{\rightleftharpoons}} (HSO_5)Mn^{III}Mn^{IV}(HSO_5) + L \quad (6c)$$

$$LMn^{III}Mn^{IV}(HSO_5) + HSO_5^- \underset{k'_{-3}}{\overset{k'_3}{\rightleftharpoons}} (HSO_5)Mn^{III}Mn^{IV}(HSO_5) + L \quad (6d)$$

$$(HSO_5)Mn^{III}Mn^{IV}L \xrightarrow{k_{ox}} X \quad (7a)$$

$$(HSO_5)Mn^{III}Mn^{IV}L + X \xrightarrow{k_{com}} 2Mn_2^{IV/IV} \quad (7b)$$

$$(HSO_5)Mn^{III}Mn^{IV}(HSO_5) \xrightarrow{k'_{ox}} X \quad (8a)$$

$$LMn^{III}Mn^{IV}L + X \xrightarrow{k_{com}} 2Mn_2^{IV/IV} \quad (8b)$$

$$LMn^{III}Mn^{IV}(HSO_5) + X \xrightarrow{k_{com}} 2Mn_2^{IV/IV} \quad (8c)$$

$$(HSO_5)Mn^{III}Mn^{IV}(HSO_5) + X \xrightarrow{k_{com}} 2Mn_2^{IV/IV} \quad (8d)$$

The experimental data could be satisfactorily simulated according to Scheme 5 (Figure 5) with minor variations in the optimized rate constants between the [**1**]-dependent data set and the $[HSO_5^-]$-dependent data set. In order to relate the observed absorbance changes to the degree of conversion of **1** to **2**, we need to know the difference in the absorption coefficients of **1** and **2** at the wavelength being followed. The constancy of absorbance at longer times (∼3 s) indicates complete conversion of **1** to **2**. Therefore, the absorbances at the start and at the end of the reaction correspond solely to the absorbances due to **1** and **2**, respectively. The difference between the two values yields the difference in the molar extinction coefficients of the two species and allows the inference of the extent of conversion from the observed absorbance changes. The calculated concentrations of **2** have been plotted in Figure 5.

The sets of rate constants from Scheme 5 that produced good fits to the experimental data have the following constraints: (1) Rate constants for the substitution of HSO_5^- by L are much smaller (∼10^6 times) than the ones for the substitution of L by HSO_5^-. This also implies that the equilibrium constants for the substitution of L by HSO_5^- are favorable (∼10^6). This is not surprising considering that HSO_5^- is much more basic (pK_a of the peroxy proton of H_2SO_5 ∼ 9) than L, which is most likely to be CH_3COO^- (pK_a of CH_3COOH ∼ 4.7), as discussed above. (2) The rate constant for the substitution of the second L by HSO_5^- is smaller, and the equilibrium constants are close to unity. Possibly, the electron density at manganese is optimal with one CH_3COO^- and one HSO_5^-, in which case the substitution of the second CH_3COO^- by HSO_5^- would lead to too high of an electron density on the manganese. (3) Substitutions on Mn^{III} have comparable or larger rate constants than substitutions on Mn^{IV}, which is expected because of the greater lability of the Jahn–Teller-distorted Mn^{III} ion. (4) The substitution of HSO_5^- on Mn^{IV} by L and the conversion of HSO_5^--bound dimers to X have comparable rate constants, and these steps are rate-determining. (5) Comproportionation of X with **1** to form **2** is extremely rapid.

The set of rate constants from Scheme 5 used to simulate the data in Figure 5 is as follows: $k_3 = (2 \pm 0.2) \times 10^6\ M^{-1}\ s^{-1}$; $k_{-3} = k'_{-3} = (4 \pm 2) \times 10^1\ M^{-1}\ s^{-1}$; $k_4 = (4 \pm 0.4) \times 10^6\ M^{-1}\ s^{-1}$; $k_{-4} = k'_{-4} = (5 \pm 0.5)\ M^{-1}\ s^{-1}$; $k'_3 = k'_4 = (4 \pm 2) \times 10^1\ M^{-1}\ s^{-1}$; $k_{ox} = (3 \pm 0.5)\ s^{-1}$; $k_{com} \geq 2 \times 10^7\ M^{-1}\ s^{-1}$. The errors and limits are based upon the tolerance of the simulations to changes in the rate constants and on the variability of the optimized rate constants between the [**1**]- and $[HSO_5^-]$-dependent data sets. The number of parameters in the simulation could be reduced by setting $k_{-3} = k'_{-3}$, $k_{-4} = k'_{-4}$, and $k'_3 = k'_4$, without affecting the closeness of the fit. The number of chemical species and steps in Scheme 5 could not be reduced, however, without the disappearance of biphasic kinetics at low $[HSO_5^-]$.

Decomposition of HSO_5^- at the pH of our study is negligible.[29,38] Moreover, HSO_5^- is in large excess, and its concentration is not directly monitored in our experiments. Thus, the decomposition of HSO_5^- was not considered in our simulations.

Note on the Simulation Procedure. Because of the relatively large number of steps and rate constants in Scheme 5, the simulation software is unable to converge to a good fit unless a reasonable set of initial values for the rate constants is provided. In particular, the biphasic behavior at low $[HSO_5^-]$ proved difficult to reproduce because most of the experimental curves are monophasic and the software is programmed to optimize the match to the greatest number of data points. It was difficult to provide a good set of initial

(37) Siegbahn, P. E. M.; Crabtree, R. H. *Struct. Bonding (Berlin)* **2000**, *97*, 125–144.
(38) Ball, D. L.; Edwards, J. O. *J. Am. Chem. Soc.* **1956**, *78*, 1125–1129.

values of the rate constants by inspection of the data because of the complexity of the mechanistic scheme. In order to overcome this problem, it was realized that the biphasic curves at low [HSO_5^-] contained a greater amount of information on the behavior of the system. Therefore, only a single biphasic curve was initially used as input data, and a simpler mechanistic scheme, with the features necessary to generate biphasic behavior, was constructed. The fitting of the biphasic curve with the simpler mechanistic scheme revealed the relative values of the rate constants necessary to generate biphasic behavior with the final scheme. The final scheme was then used to fit the reaction curves at low [HSO_5^-]. Finally, using the values of the rate constants from these fits as the initial values, the entire data set was successfully simulated (Figure 5).

Slow Ligand Exchange on Mn^{IV}. A distinctive feature of the kinetic scheme is the slow rate of exchange of HSO_5^- by L on Mn^{IV}, leading to slow interconversion between **1a** and **1b**, a condition required to rationalize the observed biphasic behavior according to Scheme 5. Although experimental data on terminal ligand exchange rates on Mn^{IV} are not available, we note that an energy barrier of 13.6 kcal mol^{-1} has been calculated for the exchange of a terminal hydroxo ligand on a mononuclear Mn^{IV} center.[33] In the same work, the barrier for exchange of a terminal oxyl ligand on $Mn_2^{IV/IV}$ with water was calculated to be 14.7 kcal mol^{-1}. In comparison, the barrier for substitution of HSO_5^- by L according to the rate constant obtained from the present simulations is 16.7 kcal mol^{-1}. The differences do not seem to be unreasonable given the differences in the identity of the ligands, the structure of the manganese complexes, and the assumption of a frequency factor equal to k_BT/h in the conversion of the rates to reaction barriers.

Slow Intramolecular Electron Transfer between Mn^{III} and Mn^{IV}. Intramolecular electron transfer between Mn^{III} and Mn^{IV} leads to interconversion between **1a** and **1b** and is required to be slow in order to account for biphasic kinetics according to Scheme 5. Rates for intramolecular electron transfer in oxo-bridged manganese complexes are not available, but an upper limit of 10^6–10^8 s^{-1} has been proposed for **3** on the basis of its EPR and near-IR absorption spectra.[31] Barriers ranging from ~13 to ~ 19 kcal mol^{-1} have been calculated by density functional theory (DFT) for $Mn^{III}(\mu\text{-}O)_2Mn^{IV}$ complexes with water, hydroxo, and formate ligands.[32] Assuming a preexponential factor of k_BT/h, these barriers translate to rates of 2400–0.1 s^{-1}.

According to the simulation of Scheme 5, the interconversion between **1a** and **1b** occurs via reactions 6a and 6b, so that the overall rate of the interconversion is limited by the rate constant $k_{-4} = 5$ s^{-1}. Electron transfer leading to interconversion of **1a** and **1b** must, therefore, be equal to, or slower than, 5 s^{-1} in order to maintain biphasic behavior according to Scheme 5. Such a rate falls within the experimental and calculated limits noted above. We also note that, whereas complexes **3** and the complexes used as models in the DFT calculation all contained identical ligand sets on the Mn^{III} and Mn^{IV} sites, the ligand sets on Mn^{III} and Mn^{IV} in complexes **1a** and **1b** are not identical. It is likely that the lack of symmetry of the ligand set in **1a** and **1b** will lead to a preference for a particular oxidation state at a given metal site, further increasing the barrier to electron transfer.

Catalysis of Water Oxidation by 1. In a study of the composition of the catalytic solution of **1** and HSO_5^-,[29] we observed that the catalytically active $Mn_2^{III/IV}$ oxidation state is present in low steady-state concentrations (~2–5% of total manganese) during catalytic oxygen evolution, while the $Mn_2^{IV/IV}$ state, catalytically inactive with HSO_5^-, is the major species (>90% of total manganese) in solution. However, once oxygen evolution stops because of depletion of HSO_5^-, the $Mn_2^{III/IV}$ state is regenerated in ~75% yield. The present proposal, that the same species X evolves oxygen upon reaction with HSO_5^- or water and that this leads to the formation of $Mn_2^{IV/IV}$ upon reaction with $Mn_2^{III/IV}$, provides an explanation for this observation.

If the reaction of X with $Mn_2^{III/IV}$ is faster than its oxygen-evolving reactions, then $Mn_2^{IV/IV}$ formation will dominate as long as there is an appreciable concentration of $Mn_2^{III/IV}$ in solution. As the concentration of $Mn_2^{III/IV}$ decreases, the rate of $Mn_2^{IV/IV}$ formation, requiring the bimolecular reaction of X with $Mn_2^{III/IV}$, slows down to a greater extent than the oxygen-evolving reaction, which is first-order in the manganese dimer. Once the concentration of $Mn_2^{III/IV}$ is depleted by conversion to $Mn_2^{IV/IV}$, then oxygen evolution via the remaining $Mn_2^{III/IV}$ species will become important. A smaller steady-state concentration of $Mn_2^{III/IV}$ also leads to a smaller amount of X and, hence, a slower rate of oxygen evolution. Once HSO_5^- is depleted, oxygen evolution slows down and the manganese in the solution is in the form of $Mn_2^{IV/IV}$, $Mn_2^{III/IV}$, and a small amount of $Mn_2^{II/III}$ (the latter being a product of the reaction of X with water).[29] $Mn_2^{II/III}$ and $Mn_2^{IV/IV}$ can then generate $Mn_2^{III/IV}$ by comproportionation.

The lack of activity of $Mn_2^{IV/IV}$ with HSO_5^- means that only a small fraction of manganese in solution is able to participate in the catalytic oxygen-evolving pathway. Hence, the maximal rate of oxygen evolution catalyzed by **1** plus oxone in a homogeneous solution is only a fraction of the potential catalytic rate. This problem could be bypassed by the use of a one-electron oxidant, which enables $Mn_2^{IV/IV}$ to form the water-oxidizing species X.[30] If two-electron oxidants are used, then $Mn_2^{IV/IV}$ formation could be minimized by use of very dilute solutions of **1** or by immobilization of **1** to prevent the bimolecular reaction of X with $Mn_2^{III/IV}$. This could be a promising direction for the improvement of **1** as a water-oxidation catalyst.[28]

Ligand Exchange and Electron Transfer between the Manganese Sites of the OEC. The exchange rates of the substrate waters with bulk water in the OEC have been measured as a means of investigating the nature of substrate binding, and the mechanism of its oxidation, at the OEC.[39] A comparison with the exchange rates in model complexes suggests that the substrates are bound terminally to metal ions in the OEC.[40,41] The exchange rates measured in the

(39) Hillier, W.; Wydrzynski, T. *Phys. Chem. Chem. Phys.* **2004**, *6*, 4882–4889.
(40) Tagore, R.; Chen, H.; Crabtree, R. H.; Brudvig, G. W. *J. Am. Chem. Soc.* **2006**, *128*, 9457–9465.

OEC span a range from 0.02 to ≥ 120 s^{-1}. Activation barriers for exchange were also measured and were in the range from 20 to ≤ 10 kcal mol^{-1}. In comparison, the calculated barriers for terminal water exchange on a $Mn_2^{IV/IV}$ dimer and terminal hydroxide exchange on a Mn^{IV} monomer are 8.6 and 13.7 kcal mol^{-1}, respectively,[33] and the barriers corresponding to the simulated rate constants for terminal ligand exchange on Mn^{III} and Mn^{IV} in Scheme 5 are in the range from 8.6 to 16.7 kcal mol^{-1} (with a preexponential factor of k_BT/h). Considering that accessibility of water to the active site is likely to add to the barrier for water exchange at the OEC, the assignment of terminal binding modes to the substrate waters in the OEC is in line with the terminal ligand exchange rates suggested by Scheme 5.

The water-oxidation site in the OEC is likely to be a manganese ion that is more oxidized than the neighboring manganese sites. In order to prevent the dissipation of oxidizing power, electron transfer between the water-oxidizing manganese and its neighbors may be required to be slow on the time scale of the water-oxidation step. The water-oxidation site has been variously proposed to be a Mn^{IV}═O adjacent to a Mn^{III} site in the S_4 state,[42] a $Mn^{IV}-O^{\bullet}$ adjacent to a Mn^{III} site in the S_3 state,[43] and a Mn^{V}═O moiety adjacent to Mn^{IV} sites in the S_4 state.[44–47] In the former cases, a high reorganization barrier is expected for electron transfer between the water-oxidizing Mn^{IV} site and the Jahn–Teller-distorted Mn^{III} site. In the latter case, an octahedral Mn^{V} water-oxidizing site would lead to a lower reorganization barrier because of a lower degree of Jahn–Teller distortion in Mn^{V} as compared to Mn^{III}, but electron exchange between a square-pyramidal Mn^{V} (a likely geometry for a Mn^{V}═O moiety[48–50]) and an adjacent octahedral Mn^{IV} would again lead to high reorganization barriers. In all cases, the manganese with the oxo or oxyl radical on it would be expected to have a preference for the higher oxidation state, leading to slow electron exchange. The effects of Jahn–Teller distortion and nonidentical ligands on the exchanging partners are, therefore, expected to be operative for electron exchange both in the OEC and in **1a** and **1b** as discussed above. The maximum electron-transfer rate constant of 5 s^{-1} ($t_{1/2} \geq 140$ ms) implied by Scheme 5 and the measured lifetimes of $\sim$200 μs and $\sim$1 ms, respectively, for the S_3 and S_4 states of the OEC[51] are consistent with slow electron transfer, leading to the existence of a localized water-oxidation site on a specific manganese in the OEC.

Conclusion

We have studied by stopped-flow UV–visible spectroscopy the kinetics of the conversion of a $[Mn^{III}(\mu\text{-}O)_2Mn^{IV}]^{3+}$ complex (**1**) to its one-electron-oxidized product, $[Mn^{IV}(\mu\text{-}O)_2Mn^{IV}]^{4+}$ (**2**), by the two-electron oxidant HSO_5^-. The kinetics of the oxidation requires the existence of an intermediate (X) between the HSO_5^--bound form of **1** and the product **2**. We propose that X is a two-electron-oxidized form of **1**, which reacts with HSO_5^- or water to produce oxygen[23] or with another molecule of **1** to produce two molecules of **2**. The $[HSO_5^-]$-dependent transition from biphasic to monophasic behavior requires the existence of two forms of **1** with different reactivities with respect to the formation of **2**. We propose that these two distinct forms of **1** represent a difference in the site of binding of HSO_5^- to **1**, with the Mn^{III}-bound form (**1a**) being able to convert to **2** via X and the Mn^{IV}-bound form (**1b**) requiring conversion to **1a** before it can react further. We are able to simulate the experimental data with a mechanistic scheme incorporating the features described above. The use of single-electron oxidants and immobilization of the catalyst are suggested as ways to improve water-oxidation catalysis by **1** in light of the proposed mechanism.

Because **1a** and **1b** can interconvert via ligand exchange or electron transfer, the kinetic distinctness of **1a** and **1b** implies that the rates of ligand exchange and electron transfer are slow on the time scale of the conversion of **1** to **2**. We note that the substrate exchange properties of the OEC and the formation of a localized water-oxidizing center in the highest S state of the OEC are consistent with the ligand-exchange and electron-transfer rates suggested by our kinetic scheme for a model $[Mn^{III}(\mu\text{-}O)_2Mn^{IV}]^{3+}$ complex and are suggestive of terminal substrate binding at the OEC.

Acknowledgment. We are grateful to Prof. Ann Valentine for help with the stopped-flow instrument. This work has been supported by the National Institutes of Health (Grant GM32715).

IC062218D

(41) Tagore, R.; Crabtree, R. H.; Brudvig, G. W. *Inorg. Chem.* **2007**, *46*, 2193–2203.
(42) Hillier, W.; Wydrzynski, T. *Biochim. Biophys. Acta* **2001**, *1503*, 197–209.
(43) Siegbahn, P. E. M.; Crabtree, R. H. *J. Am. Chem. Soc.* **1999**, *121*, 117–127.
(44) Pecoraro, V. L.; Baldwin, M. J.; Caudle, M. T.; Hsieh, W.-Y.; Law, N. A. *Pure Appl. Chem.* **1998**, *70*, 925–929.
(45) McEvoy, J. P.; Brudvig, G. W. *Phys. Chem. Chem. Phys.* **2004**, *6*, 4754–4763.
(46) McEvoy, J. P.; Gascon, J. A.; Batista, V. S.; Brudvig, G. W. *Photochem. Photobiol. Sci.* **2005**, *4*, 940–949.
(47) Isobe, H.; Shoji, M.; Koizumi, K.; Kitagawa, Y.; Yamanaka, S.; Kuramitsu, S.; Yamaguchi, K. *Polyhedron* **2005**, *24*, 2767–2777.
(48) Collins, T. J.; Gordon-Wylie, S. W. *J. Am. Chem. Soc.* **1989**, *111*, 4511–4513.
(49) Collins, T. J.; Powell, R. D.; Slebodnick, C.; Uffelman, E. S. *J. Am. Chem. Soc.* **1990**, *112*, 899–901.
(50) MacDonnell, F. M.; Fackler, N. L. P.; Stern, C.; O'Halloran, T. V. *J. Am. Chem. Soc.* **1994**, *116*, 7431–7432.
(51) Haumann, M.; Liebisch, P.; Müller, C.; Barra, M.; Grabolle, M.; Dau, H. *Science* **2005**, *310*, 1019–1021.